UNIVERSITY OF CALIFORNIA SAN DIEGO

Estimating and Controlling Droplet Displacement Induced by Local Plasma Force

A thesis submitted in partial satisfaction of the
requirements for the degree
Master of Science

in

Engineering Sciences (Mechanical Engineering)

by

Aditya A. Zadgaonkar

Committee in charge:

Professor Robert Bitmead, Chair
Professor Mauricio de Oliveira
Professor Sonia Martinez Diaz

2020

The thesis of Aditya A. Zadgaonkar is approved, and it is acceptable in quality and form for publication on microfilm and electronically:

Chair

University of California San Diego

2020

TABLE OF CONTENTS

ACKNOWLEDGEMENTS

Thank you to ASML for the privilege of working with complex and interesting machines.

Thank you to Matthew Graham, who has mentored me throughout my internship and this thesis.

ABSTRACT OF THE THESIS

Estimating and Controlling Droplet Displacement Induced by Local Plasma Force

by

Aditya A. Zadgaonkar
Master of Science in Engineering Sciences (Mechanical Engineering)

University of California San Diego, 2020

Professor Robert Bitmead, Chair

ASML is the global leader in photolithography equipment. With advent of EUV Lithography technology, it is possible to create microchips with smaller transistors and with greater precision. As EUV Lithography technology matures, customers expect ever higher productivity from these machines. This thesis analyzes a phenomenon called Local Force, which can negatively affect the system's productivity. Additionally, this thesis proposes a method to correct for the disturbances caused by the Local Force.

A set of four experiments are proposed to characterize the nature of the Local Force. These experiments demonstrate linear relation between the amount of EUV produced and the droplet displacement and impact on the upstream droplets. Additionally the experiments identify a process window in which the droplet displacement would not affect system performance.

These findings were then used to a develop Kalman predictor and a feedforward

algorithm which can compensate for the disturbances produced by the Local Force. Using data from a real machine in conjunction with a high fidelity simulation, it is shown that the algorithm can maintain the L2Dx position within the process window.

Chapter 1

Introduction

In 1965, Gordon Moore predicted that the number of transistors on an integrated circuit board would double every two years. Over the last 53 years, this prediction, which has come to be known as Moore's Law, has proven to be extremely accurate and has fueled the advancement of technology. By continuing to squeeze more transistors onto a single chip, it is now possible to carry extremely high performing devices in our pockets, which only a few years ago would have been too large and expensive for a majority of people. As of 2017, the largest transistor count on a commercial chip is 19.2 billion. To continue realizing Moore's prediction, it is necessary to develop new technologies which can provide finer resolution to meet the requirements of more advance chipsets. ASML is the global leader in producing photolithography equipment which enables the manufacturing of smaller transistors and more densely packed integrated circuits and actively works to further Moore's Law.

The modern processes of making integrated circuit chips involve a technique called photolithograhpy. In this process, a photoreactive material is spread across a silicon disk (wafer) and exposed to a precise light. Once the light interacts with the photoreactive chemical, the chemical hardens. By doping the wafer with metal and chemically treating the surface, the chip design can be built up layer by layer.

The resolution with which the light can accurately target a portion of the wafer is determined by the Rayleigh Equation. It states that the system resolution is proportional to the wavelength of light divided by the numerical aperture of the lens. $CD = \frac{k_1 \lambda}{NA}$. By reducing the wavelength, the critical dimension can also be reduced [5]. At ASML, a new light source is being developed that will produce light at $13nm$ wavelength using plasma emitted from super excited tin droplets. The produced light falls in the extreme ultraviolet regime of the electromagnetic spectrum, hence this technology is called Extreme Ultraviolet (EUV) Lithography.

As EUV technology matures, customers expect more productivity from the machines. The more wafers the customers can produce the more profit they can make. This metric is called throughput. To achieve greater throughput, the EUV source has to produce more energy and deliver a constant amount of energy to the wafer (dose). If the correct dose is not delivered (i.e. there are dose errors), the individual chipsets (dies) have to be corrected or thrown out, which affects the throughput. While there are many root causes of Dose Error, this thesis will focus on a specific type of dose disturbance caused by interaction between the plasma flash and the oncoming tin droplets, called the Local Force. It will explore an estimation based method feedforward controller to suppress the disturbance. The analysis and research done in this thesis has allowed ASML to design new algorithms which can reject Local Force disturbances. In turn, this research will allow ASML to expose wafers faster with less die loss.

Chapter 2 will explore the context and physical process of the EUV light source. Chapter 3 will introduce in detail the problem and describe and elucidate the different sensors and actuators which will be used. Chapter 4 will discuss the various tests to characterize the Local Force disturbance. Finally, Chapter 5 will utilize the data gathered in Chapter 4 to discuss the development and application of a Kalman Estimator to predict the effect of the disturbance. Additionally, it will discuss the development of a feedforward controller to correct for the Local Force disturbance.

Please note that the data in this thesis has been scaled or normalized and the units have been removed to protect ASML intellectual property. The contribution of this thesis is no way altered or impacted by these scaling. These values have been preserved for future reference.

Chapter 2

System Background

2.1 Dose

In order to maximize throughput and minimize wasted dies, it is necessary have high quality reproducible features. The process of making these features is highly dependent on the amount of energy each part of the wafer receives. This metric is called dose. Depending on the type of the photo-lithography technique being used, incorrect dose can lead to larger or smaller than expected features which can result in bad dies which must be discarded, see Figure 2.1.

Dose is defined to be the total amount of energy to which an area of the wafer is exposed. This can be expressed as

$$D = \int_0^t I(t)dt,$$

where D is the dose delivered to the wafer in mJ/cm^2 and I is the intensity of light on the wafer in mW/cm^2 [2]. The intensity of light is dependent on three major factors, the speed at which the wafer is moved (scan speed), the optics between the EUV source and the wafer, and the amount of EUV produced by the source. Light intensity is the biggest factor in Dose Stability, as the optics do not change

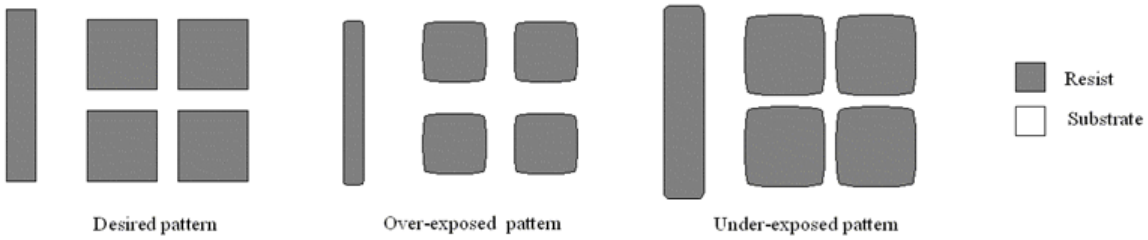

Figure 2.1: Effects of dose error on the positive dose resist. From the illustration, it can be seen that dose errors affect the size of the features on the wafer. Large errors in dose can result in mis-formed dies. Image courtesy https://www.mems-exchange.org/MEMS/processes/lithography.html.

during production and light intensity is insensitive to the scan speed as compared to sensitivity to EUV stability. Hence producing more stable EUV will yield better Dose performance.

2.2 EUV Light

The process of making Extreme Ultraviolet light starts with the production of the tin droplet. The droplet generator melts highly pure tin and produces fine stream of tin droplets. The entire process of Extreme Ultraviolet (EUV) light takes place inside a sealed vessel at near vacuum as depicted in Figure 2.2.

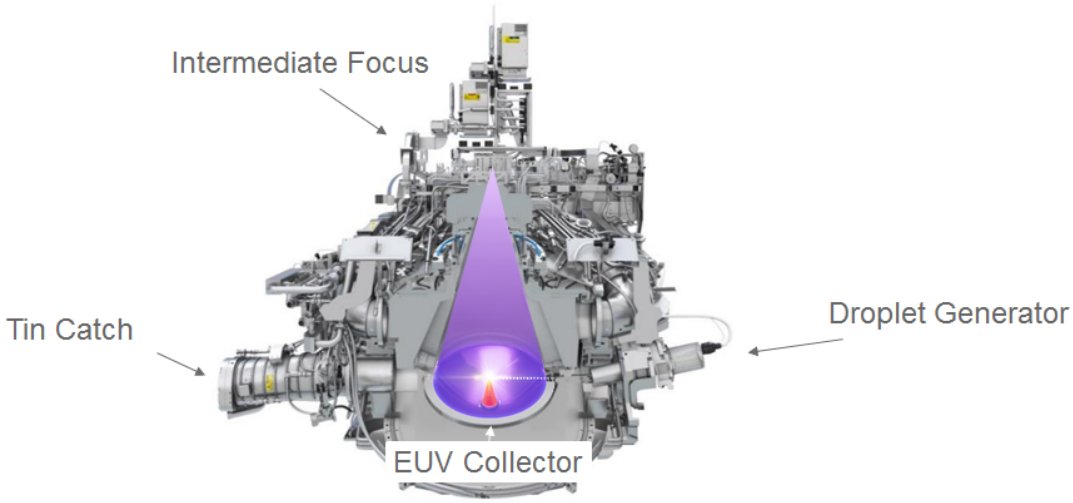

Figure 2.2: Droplets are formed using the droplet generator (device on the right) and travel towards the tin catch. As they approach the center of the vessel, the droplets are hit by a high power laser (red). The resulting EUV bounces off the collector and it focused towards the Intermediate Focus (purple)[6].

After a droplet is created, it travels across the vessel where it hit by two high power lasers. The path of the droplets is denoted as the x-axis, where the droplet generator is located on the positive side of the x-axis and the droplets move in the $-$x-axis.

The first laser (pre-pulse) hits the droplet and shapes the tin into a flat disk. The manner in which the pre-pulse laser hits the droplet affects the shape and angle of the disk [6]. The manner in which the droplet is hit is measured using a metric called the laser-to-droplet distance. This is the distance between the center of the laser to center of the droplet as shown in Figure 2.3.

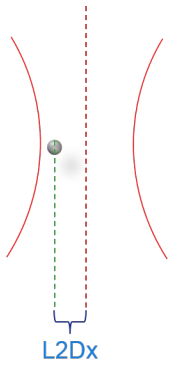

Figure 2.3: The laser to droplet distance is defined as the distance between the center of the laser beam and the center of the droplet.

Since disk shape and angle are critical elements in the production of EUV, the stability of the laser-to-droplet distance will have a direct impact on the stability of EUV [6]. In order to fire the laser accurately, a break-beam sensor is used to detect the droplet and, after a fixed time, the pre-pulse laser fires. This called the $t_{FireActual}$ delay. The L2Dx distance can also be related to the break-beam sensor.

$$\mathrm{L2D}_x = D_{drop} - D_{pp} = v_{drop} t_{Fire} - D_{pp} \tag{2.1}$$

In (2.1), D_{drop} is the distance the droplet travels from the break sensor till the pre-pulse fires, D_{pp} is the distance between the break sensor and the pre-pulse beam, and v_{drop} is the droplet x-velocity.

After the pre-pulse shapes the tin droplet, a second laser (main-pulse) blasts the tin, converting it to plasma [6]. To accurately fire the main-pulse, a second delay called the MP2PP delay is used. At the base of the vessel, there is a highly polished parabolic mirror (the collector) that focuses and reflects the light generated by the plasma towards the intermediate focus. Perpendicular to the collector is the z-axis. The collector is located on the positive side of the z-axis. Since a standard Cartesian Coordinate System is used, the y-axis is determined using the right-hand rule.

2.3 System Timing

As the droplets fly across the vessel, they pass through the Droplet Illumination Module (DIM) curtain and the break in the beam is detected by the Droplet Detection Module (DDM). The detection of the droplet by the DDM marks the time as $t_{\text{droplet crossing}}$. The DDM trigger sets off a series of timed actions to fire the lasers in the correct sequence (Figure 2.4).

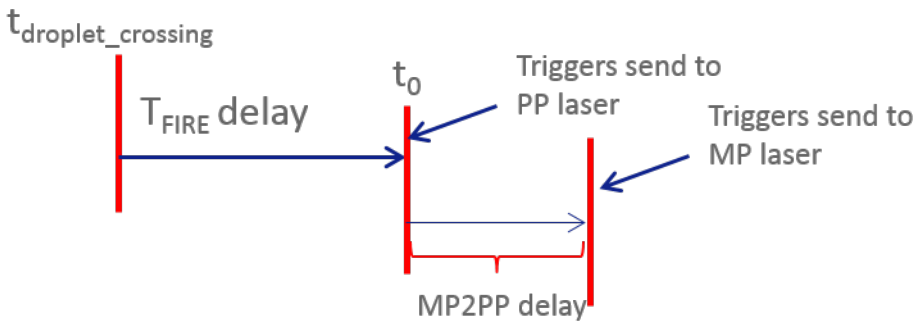

Figure 2.4: Timing Sequence diagram.

First of these actions is the pre-pulse laser firing, which occurs after the $t_{FireActual}$ delay. The $t_{FireActual}$ delay is the time between the droplet detection and pre-pulse laser firing. The delay consists of the t_{Fire} and the Local Force correction term.

$$t_{FireActual} = t_{Fire} + \Delta_{LFC} \tag{2.2}$$

The t_{Fire} term is computed by a timing controller which handles the slower disturbances (the bandwidth of t_{Fire} controller is 1000 Hz) such as pre-pulse laser drift and variation in droplets due to the droplet instability. To compensate for the faster time scale local force interaction, the Δ_{LFC} applies a correction based on the EUV value of the previous 3 shots. After the $t_{FireActual}$ delay has elapsed the pre-pulse laser fires. The $t_{FireActual}$ delay is the most critical as it determines the location of the

droplet in the laser beam, which can be referred to as the laser-to-droplet distance (Figure 2.3).

The laser-to-droplet position dictates how the droplet expands into a target for the main pulse. Perturbations in this positioning can result in lower EUV production, thereby lower system performance. For this thesis, the major focus will be on the fast time scale interaction.

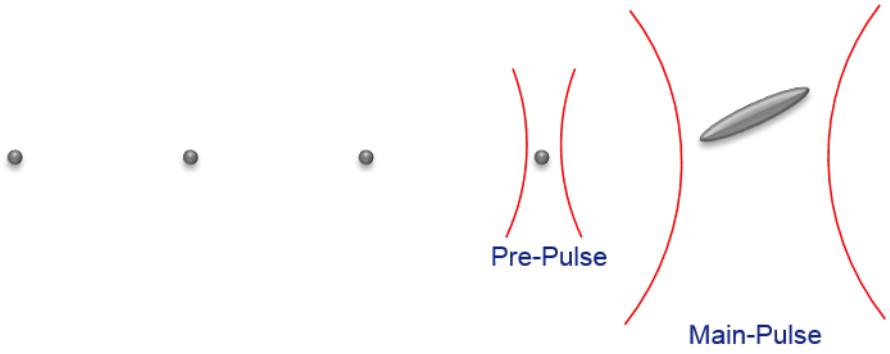

Figure 2.5: Droplet to pancake diagram.

After the pre-pulse fires, the droplet needs time to expand into the appropriate size and shape (Figure 2.5). This is called the main-pulse to pre-pulse delay (MP2PP). The MP2PP delays stays constant during steady state operation.

2.4 Timing Control

As the system operates, it is expected that there will be drifts in the laser to droplet position as there is natural variation in the droplet generation process. Since the laser-to-droplet position in the X-axis (L2Dx) has an impact on the EUV, it is important to maintain a constant L2Dx value that will ensure good EUV production. To achieve this, a feedback loop can be designed to actuate the t_{Fire} delay such that

the L2Dx value will remain within the ideal operating region. In order to measure the laser-to-droplet position, a device called a Quadcell is used to detect the position of the laser and the position of the droplet. This information is fedback into the controller to maintain a constant L2Dx value. The feedback controller has a cutoff frequency of 1000 Hz as a majority of the disturbance are slower than 1kHz.

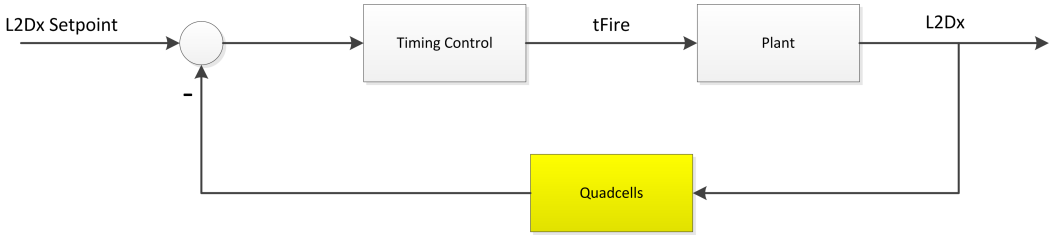

Figure 2.6: High-level overview of the timing loop controller design

2.5 Local Force

As the target is consumed by the main-pulse laser, the radiative pressure and ion emissions cause a disturbance on the upstream droplets. This disturbance manifests itself as a change in the droplet velocity and thereby causes an error of up to $15\mu m$ in the L2Dx space. The change in L2Dx causes a change in EUV which affects the performance of the system. This disturbance is called the Local Force as it only affects the local 3-5 droplets. In Figure 2.7, data was collected after many droplets were missed, thereby the only change in L2Dx is due to the Local Force. It can be seen that the Local Force's greatest impact on L2Dx displacement for the first few shots. Which in turn causes a decrease in EUV production, as seen in right plot of Figure 2.7. Repeatedly cycling the Local Force transient would cause a greater variation in EUV thereby creating unstable Dose. From the figure it can seen that the change in L2Dx displacement decays asymptotically, indicating that Local Force decays exponentially.

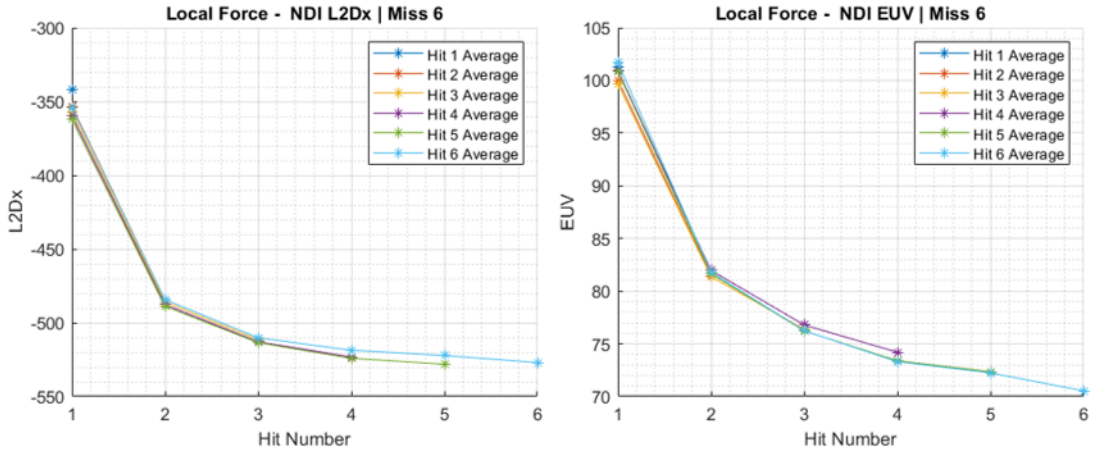

Figure 2.7: These plot above depicts change in L2Dx and EUV as the Local Force grows. Before the first point, there was no EUV being produced hence there was no effect of the local force. As more droplet are hit (Hit Number 1-6), the impact of the Local Force grows. From the left plot it can be seen that as the Local Force grows, the upstream droplets get slowed down causing L2Dx position to shift towards the droplet generator. As a result of a shift in L2Dx, there is drop in the EUV energy. During wafer production this can result in Dose Error.

The current compensation for Local Force uses the EUV produced by last three main-pulse events and computes a correction to t_{Fire} using a Finite Impulse Response logic, as describe in Equation 2.3.

$$\Delta_{LFC} = \alpha E_{k-1} + \beta E_{k-2} + \gamma E_{k-3} \tag{2.3}$$

Where Δ_{LFC} is the compensation that is applied to the t_{Fire}, E_k is the EUV produced at the k^{th} shot, and α, β, γ are calibrated gains. This correction is added to the t_{Fire} value computed by the Timing Control Controller.

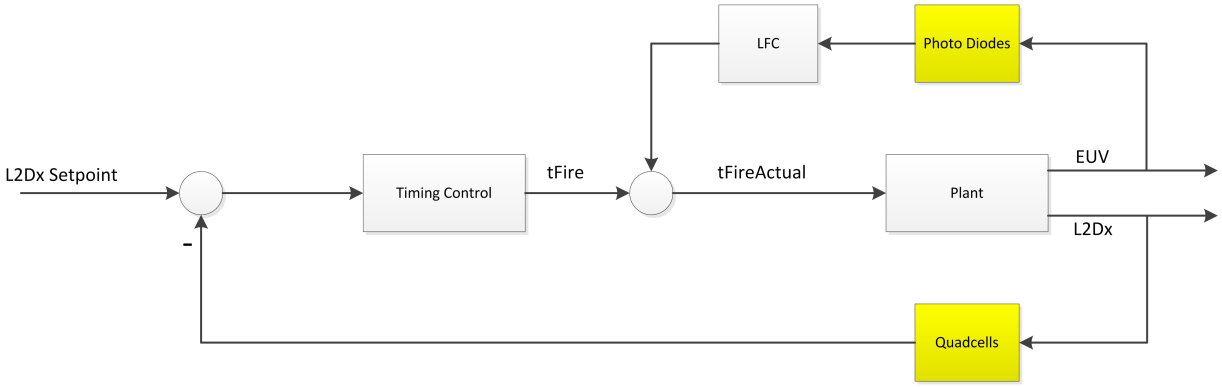

Figure 2.8: Quadcell timing loop with LFC

Since LFC does not take into account the current L2Dx location, the algorithm can under/overcompensate and push the droplet out of the operating region, if the droplets are not at the expected L2Dx location. This can be exasperated if the system drifts or the gains were set incorrectly.

To mitigate these issues an additional controller can be designed such that the correction applied would be proportional to the error in the L2Dx position. Instead an estimator can be designed to predict the effect of the Local Force on the oncoming droplets by combining the L2Dx measurements from the Quadcells and the EUV energy measurements from the Energy Sensors. Using the results from the estimator, a deadbeat controller can be designed to reject the disturbance.

Chapter 3

Sensors

On the source there are a suite of sensors for feedback control and monitoring system performance. To estimate the position of the next droplet, the intensity of EUV light is used as a proxy for estimating the Local Force and displacement associated with the Local Force is added to the current L2Dx position. The L2Dx position is measured by the Quadcells and the EUV energy is measured by the EUV energy sensors.

3.1 Quadcells

As a droplet is hit with the pre-pulse beam, it reflects part of the laser energy back into the optical path (Figure 3.1). The reflected light behaves as a point source as the droplet is near the focus of the optics. Hence, a change in the droplet position will cause the projected image to shift (Figure 3.2).

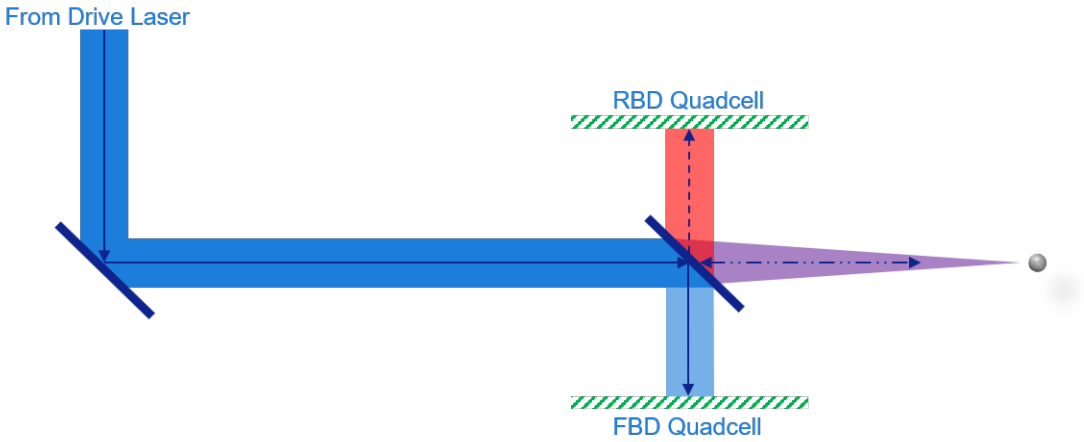

Figure 3.1: Beam Path Diagram.

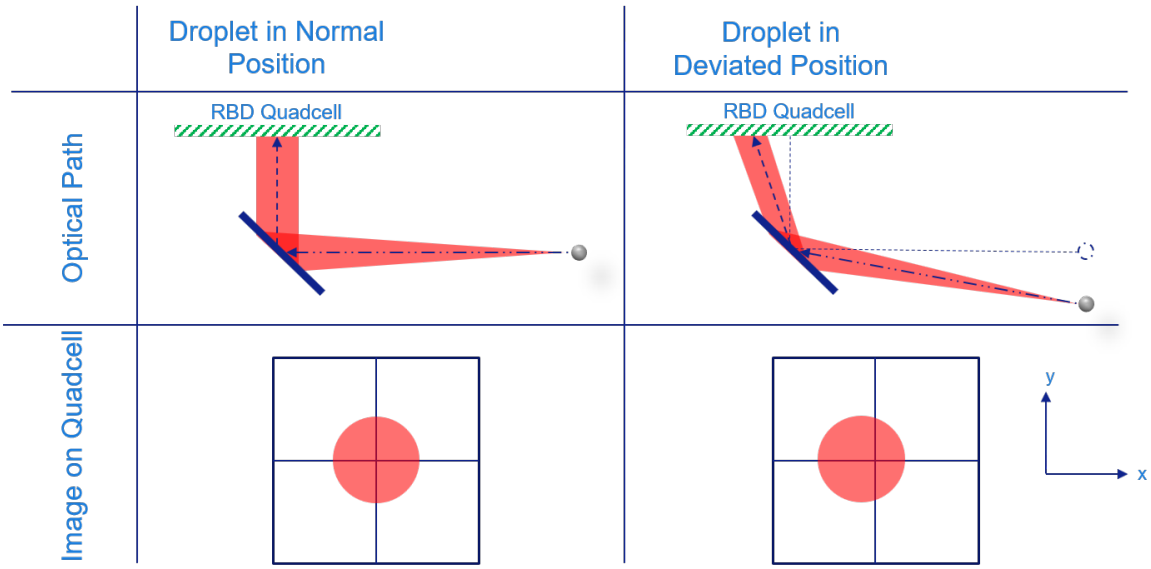

Figure 3.2: Quadcell

The reflected light is measured by a device called a Quadcell. The Quadcells

are a group of 4 photo-sensors that are designed to measure the position of the pre-laser. As mentioned in Section 2.3, there is a series of timed actions that take place after a droplet is detected. These actions also dictate the amount of time that the Quadcells see light from the laser. The ratio of the integrated voltage from each individual photo diodes can be used to compute the beam position using Equations 3.1 and 3.2. By comparing the voltages seen by the top two photo diodes with bottom two will yield the position in the Y-axis; Comparing the two left photo diodes verses the right two will yield the position in the X-axis [7].

$$QC_x = \frac{(IN1 + IN2) - (IN3 + IN4)}{IN1 + IN2 + IN3 + IN4} \tag{3.1}$$

$$QC_y = \frac{(IN1 + IN3) - (IN2 + IN4)}{IN1 + IN2 + IN3 + IN4} \tag{3.2}$$

3.2 Bisensor/EUV Sensor

Since the intensity of EUV light is being used as a proxy for estimating the Local Force, it is necessary to accurately measure the amount of EUV that is produced. In the source, it is done by collecting data using a photodiode. There are six photodiodes placed around the parameter of the collector as seen in Figure 3.3. The voltages produced by these diodes are integrated over time and scaled to report the EUV value in millijoules.

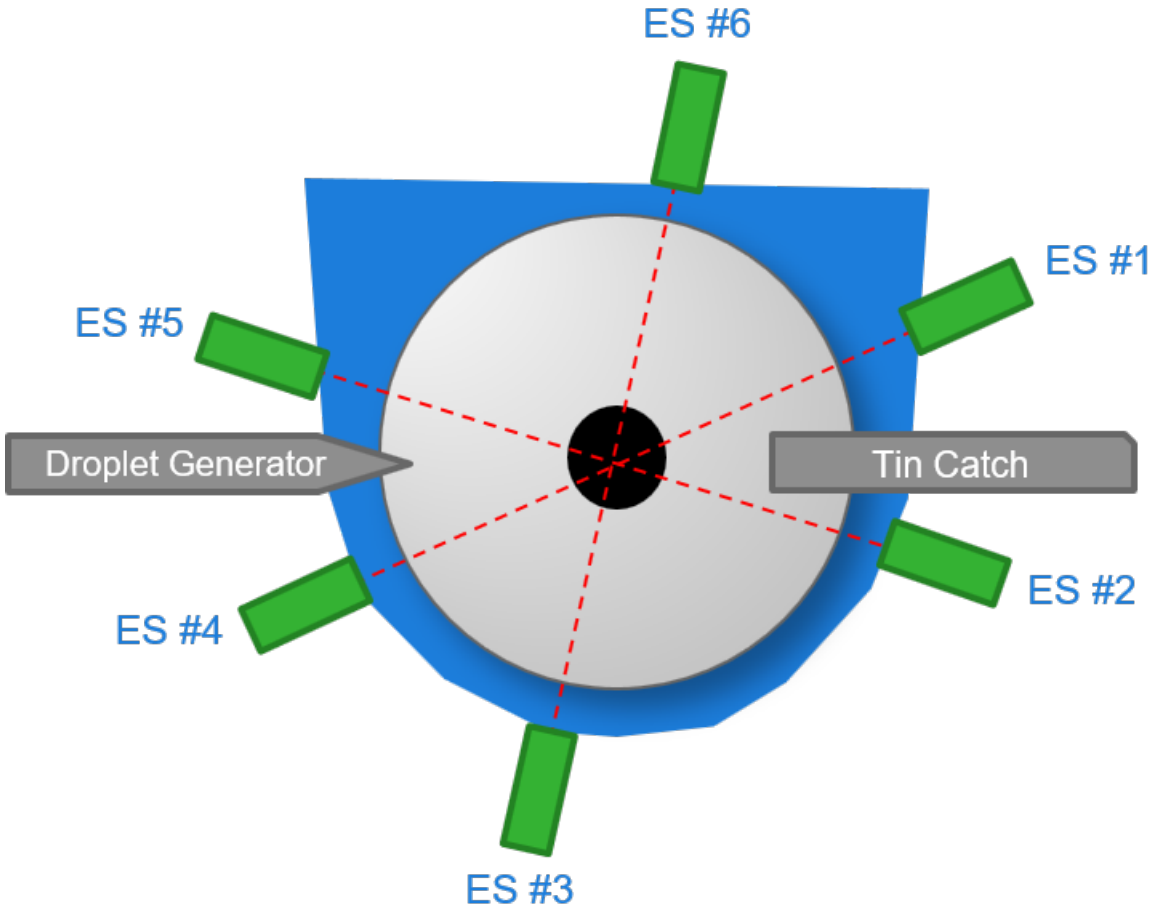

Figure 3.3: Sensor placement Diagram.

Additionally, the data from the six photodiodes can be used to observe the EUV radiation distribution in the Far Field. Leveraging similar data processing methods used on the Quad-cell, the data from the photodiodes is used to find a ratio of EUV intensity distribution along the x and y axes. These values are referred to as Bi_x and Bi_y, respectively. This Bi_x ratio might be used to further improve the quality of the estimate as it show the distribution along x-axis.

3.3 Conclusion

- The quadcell sensors can be effective in measuring the L2Dx position of the droplet
- The BiSensor measurements can be effective in measuring the directionality of EUV

Chapter 4

Modeling

In order to develop a controller to reject the local force disturbance, it is necessary to model the process and plant dynamics. For the System Identification experiment, the plant will be defined as the process and actuator between the t_{Fire} command and the resulting measured L2Dx position. The input signal will be applied to t_{Fire} and the L2Dx position will be measured as the output. To characterize the system, four sets of experimentation were performed. The first experiment was to perform a scan of the L2Dx values. This test profiles the laser to droplet space in the X-axis (L2Dx space) to characterize operating region (process window) where the magnitude of dose errors is less than 1%. The second and third sets of experimentation detail the Local Force transient as it dissipates and as the force grows by varying the number of droplets being hit and missed. The final experiment was a system identification experiment to understand the relationship between the t_{Fire} and actuator.

During modeling, the disturbances due to gas dynamics were considered negligible as they have very slow dynamics occurring on the order of seconds, whereas the Local Force occurs on the order of microseconds. Since the dynamics of the gas disturbances are 5 orders of magnitude slower than the Local Force, it can be assumed that it has an insignificant impact on the Local Force modeling.

4.1 $L2Dx$ Scan

4.1.1 Test Case Design

In the X-axis space, there is an operating region (process window) where the dose error is less than 1%. By characterizing the X-axis, the process window can be quantified so that an acceptable error range for the estimator can be found. In order to observe the effect of the droplet/pre-pulse beam profile interaction on dose/EUV, the measurements have to be taken at various laser to droplet distances. This done by changing the setpoint of the L2Dx controller. This scan was done with a range of ± 440 with a resolution of ± 90. At each scan point, data was collected for 5 seconds from the Quadcells, and EUV sensors.

4.1.2 Test Results and Analysis

Since the metric for measuring the process window is the magnitude of dose error, the measured EUV data has to be post processed to calculate dose and the deviation from the target dose. As the laser beam shines on a finite area while the wafer is in motion, the dose on the wafer can be calculated by performing a convolution of the beam profile on wafer and the EUV signal. To simplify the calculation, the beam is approximated to be a trapezoid. The plot of the laser to droplet position versus the dose error can be visualized using a collection of histograms for each laser-to-droplet position.

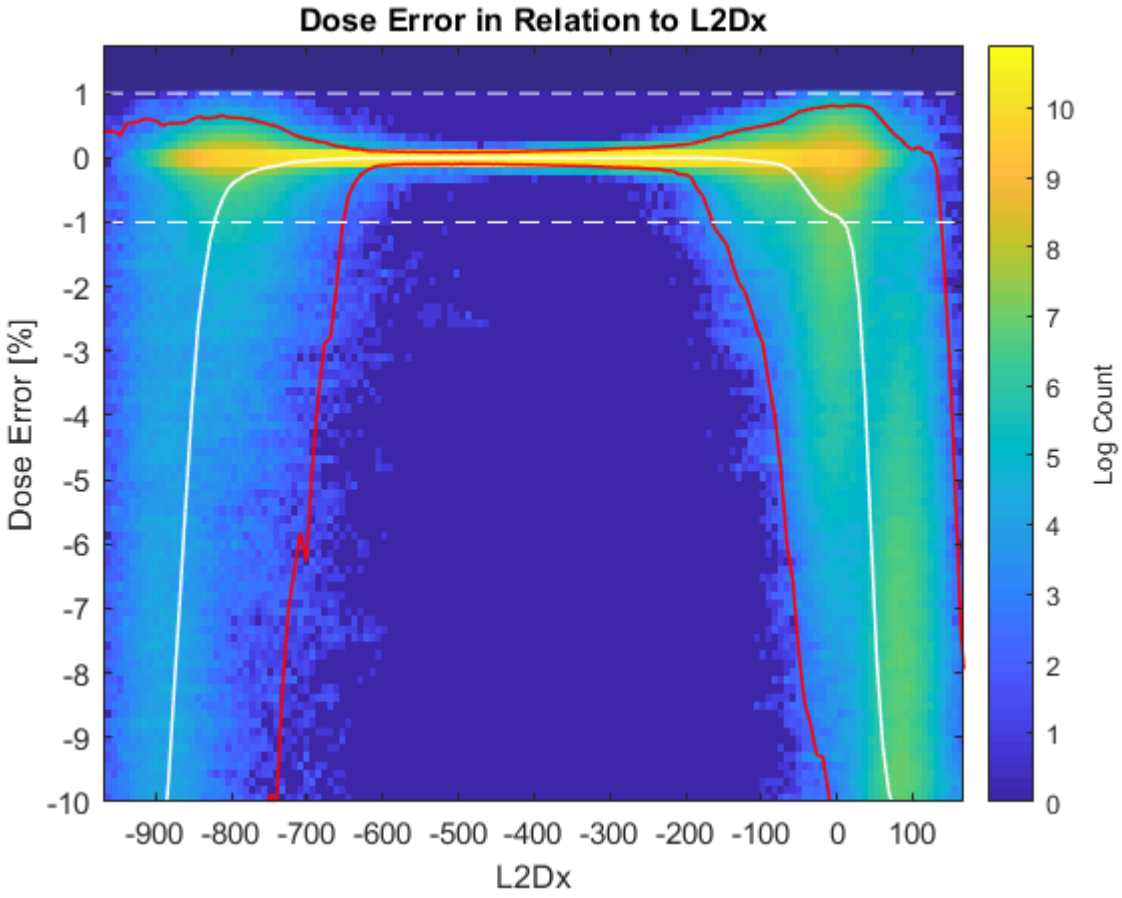

Figure 4.1: The plot above depicts dose errors versus different laser to droplet position. With this data set, the operating region in the L2Dx space can be seen. Between L2Dx of -525 and -225 the dose errors are less than 1%

From Figure 4.1, it can be seen where dose errors are most prevalent. Since the machine specification calls for less than 1% dose error, that will be the condition to characterize the process window. From Figure 4.1, it can be seen that the process window is 300 wide. Since the normal operating condition is 300, the acceptable error the estimator is ± 150.

Conclusions

- The estimator must have an error less than ±150 to fit within the process window

4.2 Local Force Growth Transient

4.2.1 Test Case Design

To develop a model for the effect of the Local Force, it is necessary to quantify the deceleration of the droplets due to Local Force. This experiment will explore the linearity between EUV and droplet displacement and the extent of the Local Force. This effect can be observed by measuring the laser to droplet displacement transient after a period of off-droplet shots. Additionally, it is necessary to measure the effect that previous Local Force events have on the deceleration. By varying the number of off-droplet shots and on-droplet shots, the varying effect of Local Force on deceleration can be captured. For this experimentation, the number of droplets hit were varied between 1-6 and the number of missed droplets were varied between 1-6. This pattern can be repeated over 5 seconds to get a larger sample size. The droplet frequency is 50 kHz, therefore approximately 12,500 samples will be collected.

4.2.2 Test Results and Analysis

Since there are tens of thousands of samples being collected, the laser-to-droplet positions have to be centered. The trend in the data can then be observed as an average with 99.7% and 0.3% bounds, as represented by the red dashed line and the green dashed line, respectively. To center the plot, the first laser-to-droplet position measurement is subtracted from the packet to remove the bias in the data.

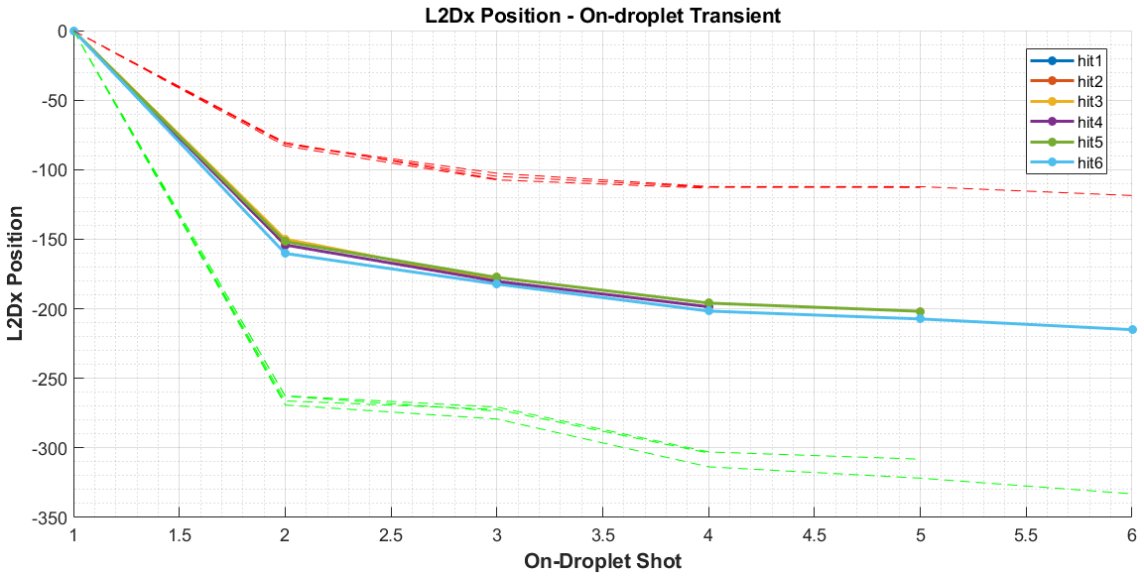

Figure 4.2: Plot of the Local Force growth transient. This plot using data from with 6 missed droplets. From this plot, it can be seen that the transient only lasts for the first 2-3 droplets. The dashed red and green lines represents the 99.7% and 0.3% percentile.

From analyzing this plot (Figure 4.2), it can be concluded that the first droplet after the local force event will see the largest impact on the position. The additional droplets will see a substantively lower impact on the disturbance. From the percentile bounds, it can be seen that there is a large spread in the L2Dx displacement. From previous studies, it is believed that these variations are due to the natural variation in EUV. To validate this hypothesis, the droplet k's EUV can be plotted against the droplet $k+1$'s L2Dx position.

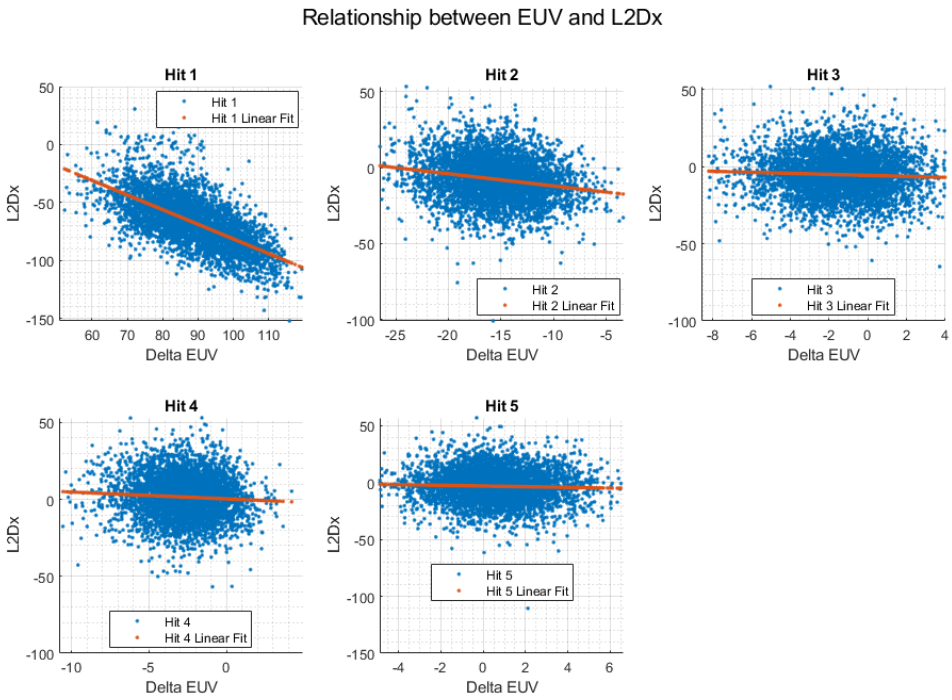

Figure 4.3: Relationship between EUV and L2Dx for on-droplet transient

In Figure 4.3, it can be seen that there is a linear relationship between the EUV produced by the Local Force event and the Laser to Droplet displacement. A line can be fitted through the data to produce a linear sensitivity. With these plots it can be seen that after the 2nd shot there a is lower sensitivity of EUV to L2Dx displacement.

Conclusions

- Local Force compounds at a different rate from the Local Force decay, therefore the state estimation model changes depending on whether the droplet was hit or missed.

4.3 Local Force Decay Transient

4.3.1 Test Case Design

Similarly to the pattern that was developed in the previous section, a pattern can be developed to observe the acceleration caused by the absence of the Local Force. To develop a model for the effect of the Local Force, it is necessary to quantify the acceleration of the droplets in absence of the Local Force.

Since the change in velocity is to be observed, it is necessary to measure the laser to droplet position, as a velocity change will directly manifest itself as a change in the droplet position. This can be accomplished by creating a Local Force event (i.e. hit the droplet with the main-pulse) and measuring the laser to droplet position of subsequent droplets. The laser to droplet distance can only be measured if the droplet is hit by the pre-pulse laser. Since the pre-pulse and main-pulse lasers cannot be fired independently, the droplet of interest has to also be hit by lasers. After the droplet is hit, ten droplets were missed to dissipate the Local Force caused by measuring the position of the droplet. The pattern for observing the Local Force effect on the first droplet is visualized in Figure 4.4.

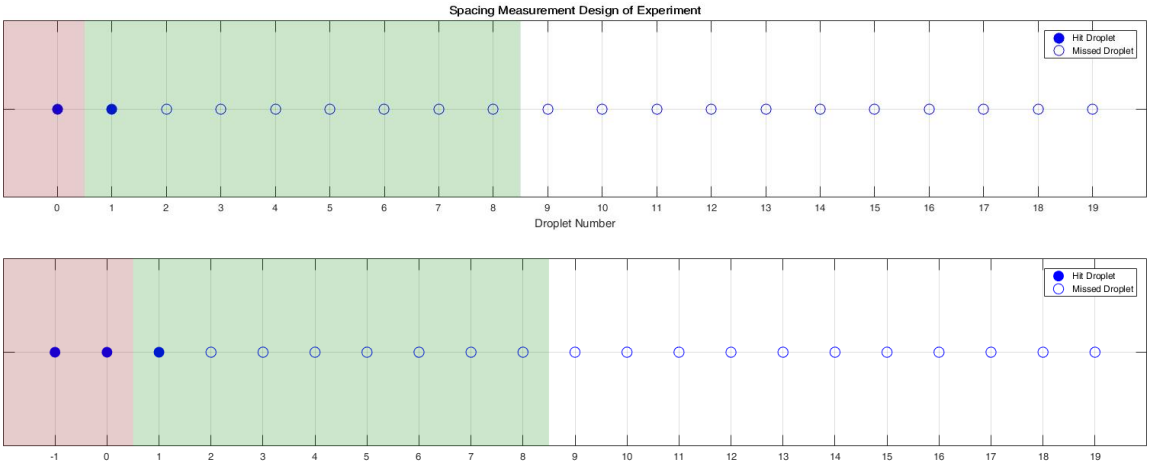

Figure 4.4: Design of Experiment for Local Force Decay Transient. A closed circle denotes a hit droplet. A open circle denotes a missed droplet. The red highlighted section represents the droplets which are hit for inducing the local force. The green highlighted section represents the droplets which are hit for measurement.

This pattern can be further extended to observe the impact of multiple Local Force events by hitting more droplets before the measurement phase. Similarly to the previous test, the patterns can be repeated to get a larger sample size. Additionally, similar data can be used to validate the estimator.

4.3.2 Test Results and Analysis

Similarly to the previous test there are tens of thousands of samples collected, so it was most appropriate to recenter the laser to droplet position to the Local Force causing droplet and observing the data as an average with 99.7% and 0.3% bounds. To recenter the plots, the first laser-to-droplet position measurement is subtracted from the packet to remove the bias in the data. Each of the separate test points can be collated into one graph as seen in Figure 4.5

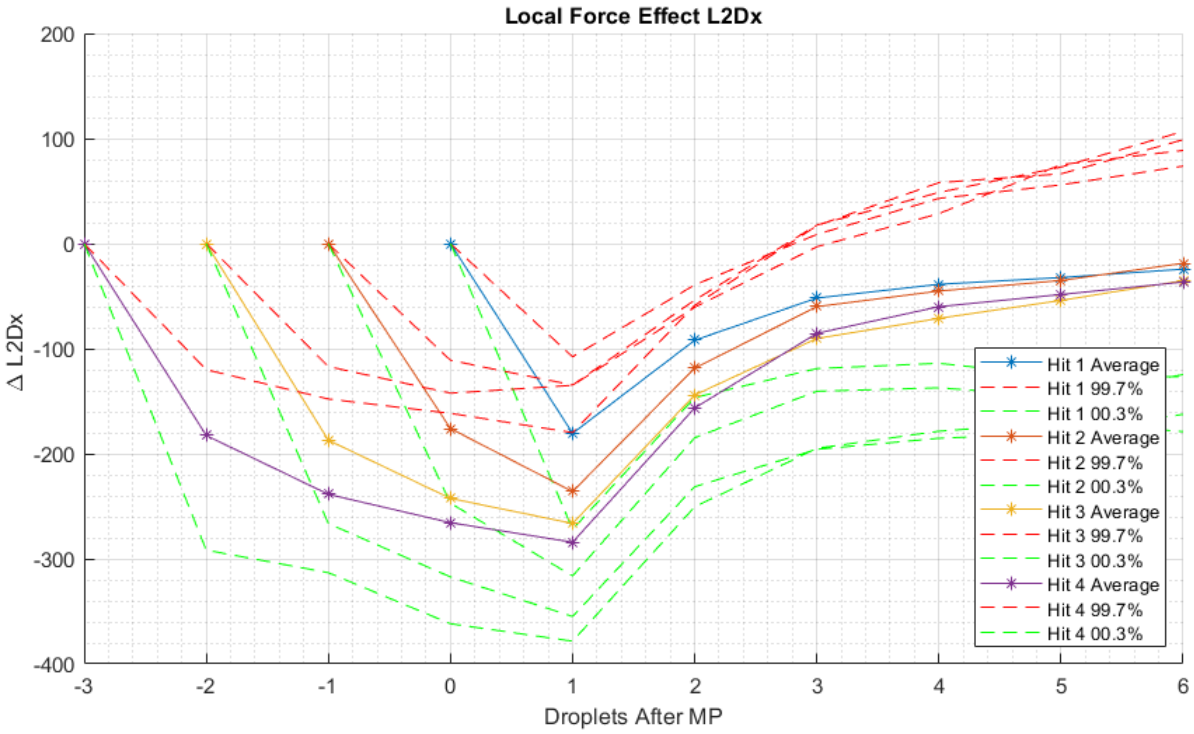

Figure 4.5: Plot of Local Force decay. The negative and zero droplet numbers represents the droplets hit to induce the Local Force. Positive numbers indicate the droplets after the last Local Force Inducing droplet hit.

To visualize the the effect of the local force, the measured laser to droplet position is taken as displacement from the initial local force event. In the above plot (Figure 4.5), the negative and zero "Droplet After MP" represents the hit droplets and positive "Droplet After MP" represents the missed droplets. From analyzing the plot (Figure 4.5), it can be concluded that the first droplet after the local force event will see the largest impact on the L2Dx position. The additional droplets will see a substantively lower impact on the droplet position. Additionally, it can be see that the effect of the Local Force extends to the 3rd droplet past the Local Force Event. After the 4th droplet, there is little change in the displacement of the droplets as

demonstrated by the purple and yellow lines. Similarly, the off-droplet transients decays after the 3rd droplet. For simplicity the model can be truncated to the first three droplets. The assumption that the disturbance in the laser-to-droplet position is proportional to the energy of the main pulse laser can be validated by plotting the displacement against EUV.

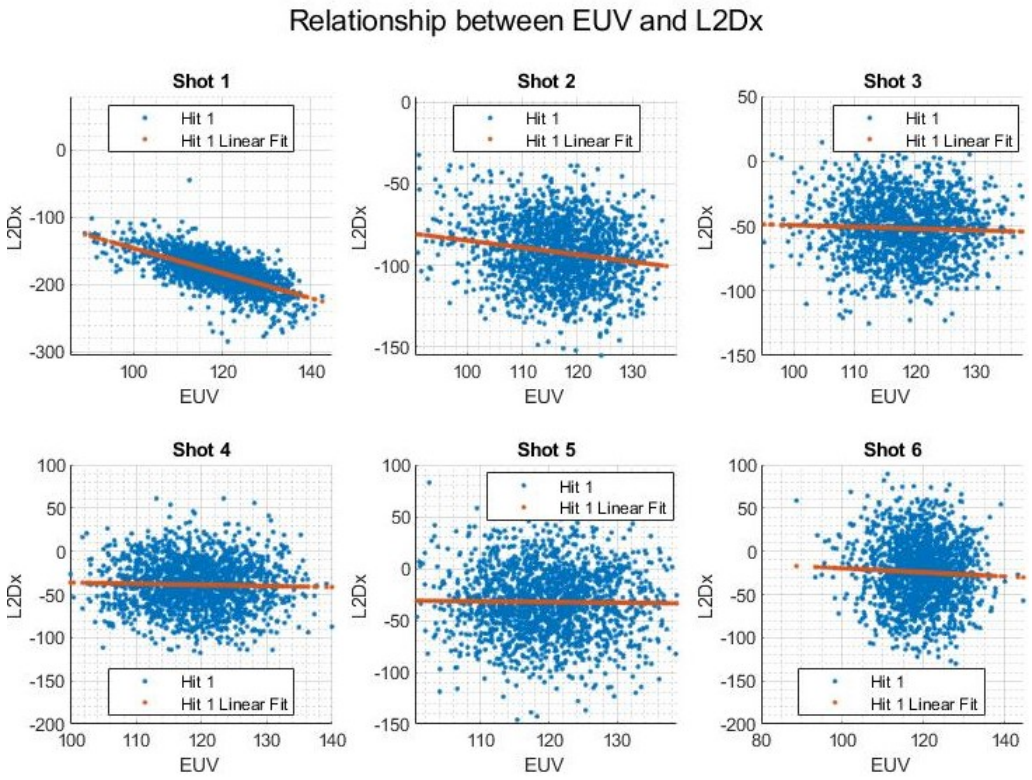

Figure 4.6: Relationship between Local Force Event EUV and Droplet displacement

In this figure, it can be seen that there is a linear relationship between the EUV produced by the Local Force event and the Laser to Droplet displacement. A line can be fitted through the data to produce a linear sensitivity. With these plots it can be confirmed that after the 4th shot there is no more sensitivity of the Local Force EUV to Laser to Droplet displacement.

Similar to the analysis done in Figure 4.3, an analysis can be made for the relationship between the bi-sensor measurement by the Local Force event and the Laser to Droplet displacement as seen in Figure 4.7.

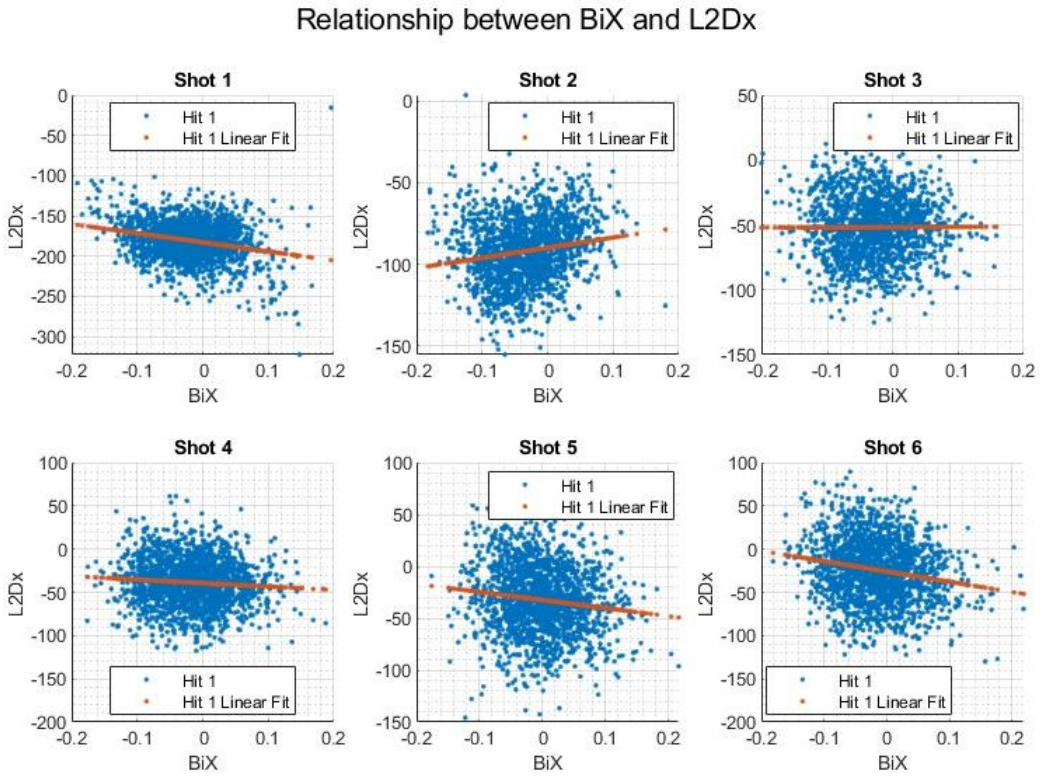

Figure 4.7: Relationship between Local Force Event EUV and BiX

However, it can be seen from the figure that there is little sensitivity between BiX and Laser to Droplet displacement. Therefore, it can be concluded that the Bi-Sensor measurement is not significant for the Local Force modeling.

Conclusions

- The Local Force mostly dissipates after 3 droplets so the model only needs to keep a record of the past 3 droplets
- The Displacement in L2Dx is linear with respect to EUV, hence a linear estimator can be designed
- There is no correlation between Bi-Sensor X and the L2Dx displacement

4.4 Empirical Transfer Function Estimate

4.4.1 Test Case Design

Finally to understand the dynamics of actuator, i.e. the dynamics between the t_{Fire} delay and the laser to droplet position, an Empirical Transfer Function Estimate (ETFE) experiment can be devised. Since delaying the pre-pulse will result in the droplet traveling farther at constant velocity, the relationship is expected to be constant. That is, there will not be any poles or zeros in the output of the ETFE. The result of this test will help validate that there are no additional dynamics in the system.

By injecting frequencies of interest into the t_{Fire} input and comparing to the frequencies at the output by measuring L2Dx position, the dynamics of the actuator can be found. The results of this experimentation can be used to develop a deadbeat feedback controller to eliminate the disturbances. For this experiment, a multiple probes were injected into the system as seen below.

- Multi-sine 1-40Hz with spacing for 1 Hz
- Chirp Signal from 20-200Hz
- Chirp Signal from 100-600Hz

- Chirp Signal from 500-2000Hz
- Chirp Signal from 1000-10000Hz

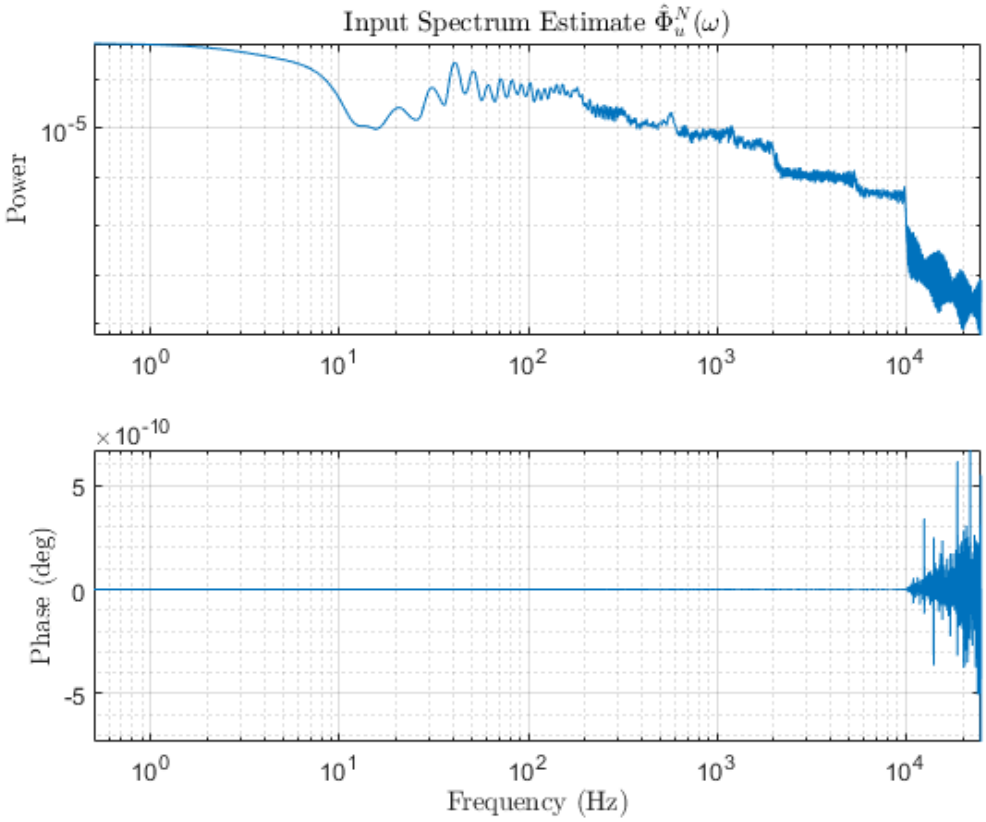

Figure 4.8: Input Signal ETFE.

4.4.2 Test Results and Analysis

The ETFE calculation as described in Equation 4.4 [4].

$$y(t) = G(q)\,u(t) + v(t) \tag{4.1}$$

$$\mathcal{L} \downarrow$$

$$Y_N(\omega) = G\left(e^{j\omega}\right) U_N(\omega) + V_N(\omega) \tag{4.2}$$

$$\hat{\hat{\Phi}}_{yu}^{N} = \frac{1}{N} Y_N(\omega)\,\overline{U_N(\omega)} \tag{4.3}$$

$$G_{ETFE} = \frac{\int_{\zeta=\pi}^{\pi} \hat{\hat{\Phi}}_{yu}^{N}(\zeta)\, w(\omega-\zeta)\, d\zeta}{\int_{\zeta=\pi}^{\pi} \hat{\hat{\Phi}}_{u}^{N}(\zeta)\, w(\omega-\zeta)\, d\zeta} \tag{4.4}$$

Since it is known that there is a 1 shot delay between $t_{FireActual}$ and the laser firing, the data is shifted to remove the delay. Additionally the off-droplet shots are also removed as collected data during this time is just noise.

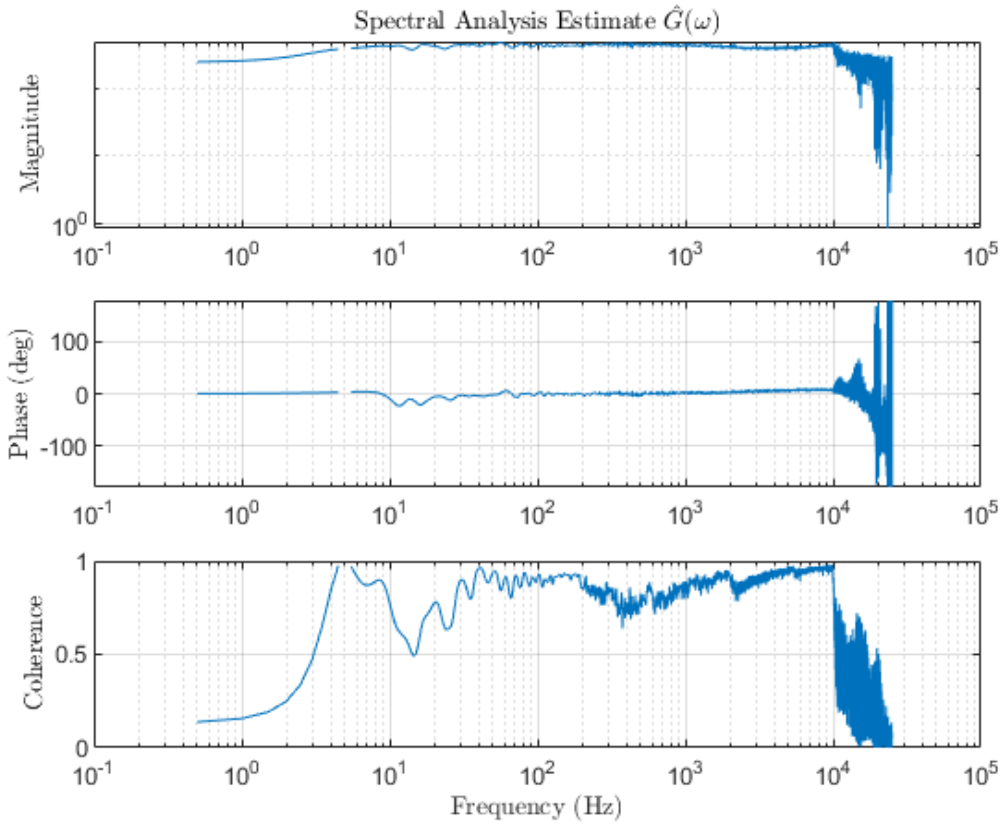

Figure 4.9: Output of ETFE.

From the System Identification Test as seen in Figure 4.9, it is seen that the system transfer function is a static gain of ~ 439 with no poles or zeros in the system. Beyond 10kHz, the coherence of the test drops, indicating that other internal forces are causing disturbances at that frequency. Additional testing with a high frequency random probe, confirmed that there no poles at the higher frequency From the phase plot of the ETFE Output (Figure 4.9), it seem that it is decaying linearly with frequency, which would indicate an additional delay in the system.

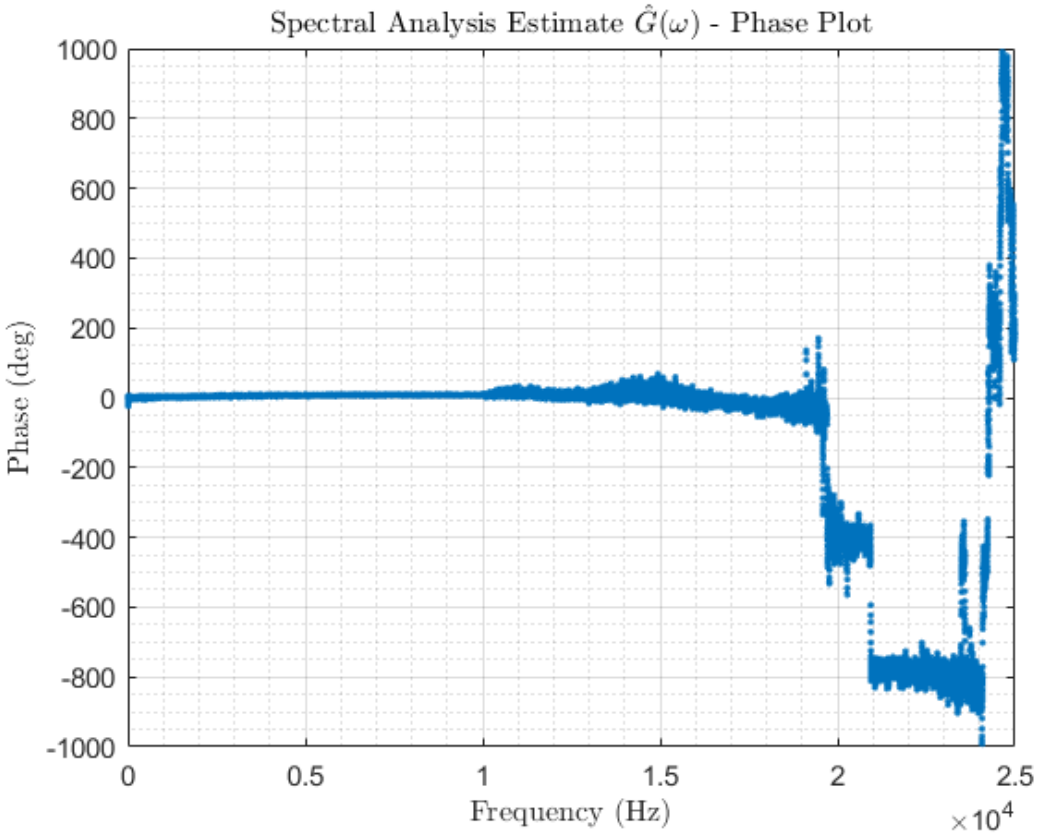

Figure 4.10: Output of ETFE.

However, plotting the phase as a linear plot revels that the phase is not decaying linearly with frequency in the region of interest(Figure 4.10). Indicating that there are no additional delays in the system. The final transfer function can be denoted as $\frac{-439}{z}$.

Conclusions

- ETFE shows that there is a delay between t_{Fire} and L2Dx and no additional dynamics. Test shows that the droplets are traveling at the constant speed
- A deadbeat controller in t_{Fire} can be designed to correct the disturbance in the

L2Dx position.

Chapter 5

Design of the Kalman Predictor and Feedforward Controller

With the data collected in the previous chapter, it is possible to create a state estimator to estimate the droplet position relative to the pre-pulse laser. Once the laser to droplet distance can be predicted, it can be used to create a feedforward controller to eliminate the Local Force Transients. This chapter will discuss the design of the state estimator and the feedforward controller.

5.1 Feedforward Controller

The goal of the controller is to maintain a constant L2Dx in the presence of the Local Force disturbance by manipulating the tFire values. This control problem can be expressed as the following state-space representation.

$$\delta_{k+1} = \delta_k + Bu_k + w_k \tag{5.1}$$

$$y_k \quad = \delta_k \tag{5.2}$$

Excluding the disturbance caused by the Local Force, the L2Dx position does not vary with time. Therefore, the state transition matrix can be expressed as an

identity matrix. The System Identification experimentation (Chapter 4) showed that the relationship between tFire to L2Dx is $\frac{439}{z}$. Hence control input matrix, B, is 439. The L2Dx position is subject to the disturbance caused by the Local Force; this disturbance is represented by w_k in 5.1. As the L2Dx position can be directly measured by the quadcells, the output matrix is also an identity matrix. If the value of w_k can be predicted, then a minimum variance controller can be designed to correct for the effect of the Local Force.

A prediction of the disturbance caused by the EUV generated by the last three shots is required to accurately track droplet position and ultimately correct for the Local Force disturbance. A state space model was chosen to represent this phenomenon as it could track the disturbances in droplet velocity over time. Change in EUV energy has the greatest correlation with the disturbance in the droplet position (Chapter 4). The upstream droplet position is estimated by summing the L2Dx disturbance to the current L2Dx position

$$\delta_{k+1} = \delta_k + Bt_{Fire_k} + w_k(t_{Fire_k}) \tag{5.3}$$

where δ_k is the laser-to-droplet position of the k^{th} droplet. The disturbance in laser-to-droplet position is a cumulative change in droplet velocity multiplied by the t_{Fire} value

$$w_k = t_{Fire_k} * (\Delta\nu_k^1 + \Delta\nu_k^2 + \Delta\nu_k^3) \tag{5.4}$$

where $\Delta\nu_k^j$ is the velocity change of droplet k due to the Local Force caused by preceding droplet at time $k - j$. From the analysis in Chapter 4,

$$\Delta\nu_k^1 = \alpha_{k-1}\Delta E_{k-1}, \tag{5.5}$$

$$\Delta\nu_k^2 = \beta_{k-2}\Delta E_{k-2}, \tag{5.6}$$

$$\Delta\nu_k^3 = \gamma_{k-3}\Delta E_{k-3}, \tag{5.7}$$

where α_k, β_k, and γ_k are scalar values that translate the change in EUV to the change in droplet velocity, and $\Delta E_k = E_k - E_{k-1}$ where E_k is the EUV at the k^{th} time-step.

$$\therefore w_k = t_{Fire_k} * (\alpha_{k-1}\Delta E_{k-1} + \beta_{k-2}\Delta E_{k-2} + \gamma_{k-3}\Delta E_{k-3}) \tag{5.8}$$

The model incorporates the last three values of ΔE as the EUV produced at the k^{th} time step will affect the next three droplets. This equation can be re-written as state-space model with the states

$$x_k = \begin{bmatrix} \delta_k \\ \Delta E_{k-1} \\ \Delta E_{k-2} \\ \Delta E_{k-3} \end{bmatrix}. \tag{5.9}$$

In state space,

$$\begin{aligned} \begin{bmatrix} \delta_k \\ \Delta E_k \\ \Delta E_{k-1} \\ \Delta E_{k-2} \end{bmatrix} &= \begin{bmatrix} 1 & \alpha_{k-1}\text{tFire}_k & \beta_{k-2}\text{tFire}_k & \gamma_{k-3}\text{tFire}_k \\ 0 & 0 & 0 & 0 \\ 0 & 1 & 0 & 0 \\ 0 & 0 & 1 & 0 \end{bmatrix} \begin{bmatrix} \delta_{k-1} \\ \Delta E_{k-1} \\ \Delta E_{k-2} \\ \Delta E_{k-3} \end{bmatrix} \\ &+ \begin{bmatrix} 439 \\ 0 \\ 0 \\ 0 \end{bmatrix} t_{Fire_k} + \begin{bmatrix} 0 \\ 1 \\ 0 \\ 0 \end{bmatrix} \Delta E_k. \end{aligned} \tag{5.10}$$

The values of α_k, β_k, and γ_k can be extracted from the slopes derived in the previous chapter. Since it was found that the on-droplet verses the off-droplet transients were different, the control-input model will have to change based on whether the system is firing on verses off droplet. The final derived model can be seen in Equation 5.11 for the on-droplet case and Equation 5.12 for the off-droplet case.

$$\begin{cases} \alpha_k = -0.0826 \\ \beta_k = -0.0525, \quad k \in \text{OnDroplet} \\ \gamma_k = -0.0216 \end{cases} \tag{5.11}$$

$$\begin{cases} \alpha_k = -0.0884 \\ \beta_k = -0.0545, \quad k \in \text{OffDroplet} \\ \gamma_k = -0.0274 \end{cases} \tag{5.12}$$

Finally the only output that can be observed is the laser to droplet position and the change in EUV. Hence the H matrix can be written as $\begin{bmatrix} 1 & 0 & 0 & 0 \\ 0 & 1 & 0 & 0 \end{bmatrix}$.

$$y_k = \begin{bmatrix} 1 & 0 & 0 & 0 \\ 0 & 1 & 0 & 0 \end{bmatrix} x_k \tag{5.13}$$

This yields a non-linear time varying estimation problem, which is observable as long as t_{Fire} is non-zero. Since the control value of t_{Fire_k} is known along with ΔE_k, these values can be substituted into the equation and the non-linear time varying estimator becomes a time varying linear estimator.

A Kalman Estimator algorithm was chosen as it is the most optimal estimator for a state space model with Gaussian noise distribution. The original derivation of the filter can be found in [3]. Additionally the Kalman Estimator can quantify the uncertainties caused by other within the source. The Kalman filter takes the form of

$$x_{k+1} = F_k x_k + B_k u_k + w_k \tag{5.14}$$

$$y_k = H_k x_k + J_k u_k + v_k \tag{5.15}$$

$$\begin{bmatrix} x_0 \\ w_k \\ v_k \end{bmatrix} \sim \mathcal{N}\left(\begin{bmatrix} \hat{x}_{0|-1} \\ 0 \\ 0 \end{bmatrix}, \begin{bmatrix} P_{0|-1} & 0 & 0 \\ 0 & Q_k & 0 \\ 0 & 0 & R_k \end{bmatrix} \right) \tag{5.16}$$

where x_k is the state of the system, F_k is the state transition matrix, u_k is the control input, B_k is the control-input model, and w_k is the process noise. In the measurement equation y_k is the measurement, H_k is the observation matrix, J_k is the feedthrough matrix, and v_k is the measurement noise. The $P_{k|k-1}$, Q_k, and

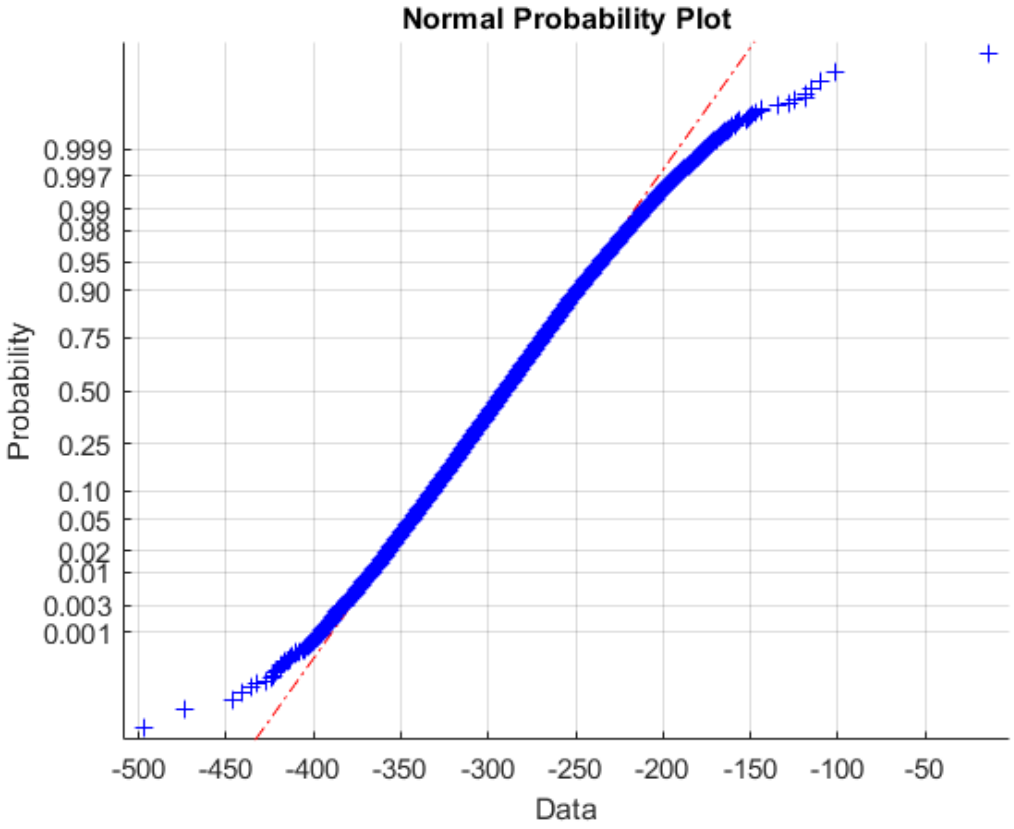

Figure 5.1: Normal distribution test of L2Dx data. The noise distribution of the Laser-to-droplet is Gaussian

R_k, matrices represent the covariances of the state, process noise, and measurement noise, respectively [8]. For this application of the Kalman Filter, the control input is the tFire value computed by the Timing Control and the output measurement is the measured L2Dx value, as mentioned in the Chapter 4. The change in velocity must be accounted for when estimating the L2Dx position. Hence, the velocities of the upcoming droplets are the states of the model.

Since the laser-to-droplet position is controlled by a PI controller during normal operation, the 3 sigma distribution of laser-to-droplet position can be predicted by

the controller design. Covariance is computed as the standard deviation squared. Therefore $E\left[(x-\hat{x})^2\right] = \sigma^2 = 146.3$ and, the variable $P_{0|-1}$ can be assigned a value of 146.3. When the system operates in open-loop, the error between the droplet position and desired laser-to-droplet position has a 3 standard deviation value of 398.35. By the design of the laser-to-droplet controller, the system is expected to have a $2.7dB$ attenuation therefore the expected 3 standard deviation is 292.60. Additionally, laser-to-droplet controller will reduce the disturbance to within 3 standard deviation of 292.60. Therefore the variance of L2Dx is $9,512.75$. From the experimentation it Chapter 4, it is know that the change in EUV has a standard deviation of 50.12. Therefore EUV has a variance of 2511.90. From these values Q_k can be constructed.

$$Q_k = \begin{bmatrix} 9,512.75 & 0 & 0 & 0 \\ 0 & 2511.90 & 0 & 0 \\ 0 & 0 & 2511.90 & 0 \\ 0 & 0 & 0 & 2511.90 \end{bmatrix} \tag{5.17}$$

Using the output of the Kalman Filter, it is now possible to construct a minimum variance controller to eliminate the disturbance caused by the Local Force [1].

$$\delta_k = \delta_{k-1} + Bt_{Fire_{k-1}} + w_k(t_{Fire_{k-1}}) \tag{5.18}$$

$$\hat{\delta}_{k|k-1} = \delta_{k-1} + \text{tFire}_k\left[439 + \Delta\nu_k^1 + \Delta\nu_k^2 + \Delta\nu_k^3\right] \tag{5.19}$$

The minimum variance control law is

$$\text{tFire}_k = -\frac{\delta_{k-1}}{439 + \Delta\nu_k^1 + \Delta\nu_k^2 + \Delta\nu_k^3}.$$

Incorporating the minimum variance controller to the state estimator, the final system design can be found in Figure 5.2.

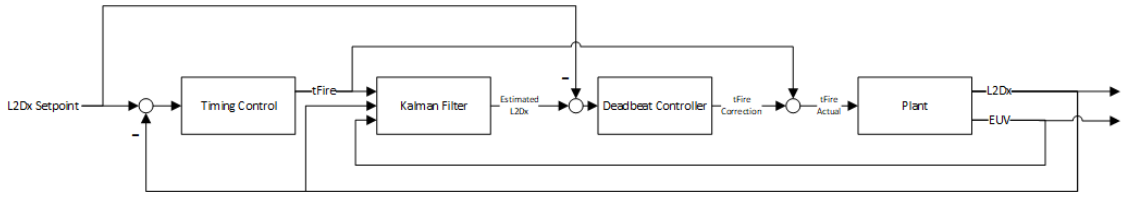

Figure 5.2: Feedforward Diagram

5.2 Estimation Validation

The design was validated by using a high fidelity MATLAB simulation with real data from the source. The validation set consisted of the data similar to the Local Force Growth Transient test case. By using this data, it was possible to validate the estimator for the various Hit/Miss test cases. The algorithm consists of two part: the Time-Update and the Measurement Update. The Time Update updates the prediction of the state estimation and the prediction of the co-variance matrix. The Measurement Update updates the states and the covariance matrices based on the quadcell measurements. The equation for Time Update can be found in Equation 5.20 - 5.22. The equation for Measurement Update can be found in Equation 5.23 - 5.25.

$$\hat{x}_{k+1|k} = F_k \hat{x}_{k|k} + G_k \Delta E_k + B_k u_k \tag{5.20}$$

$$P_{k+1|k} = F_k P_{k|k} F_k^T + Q_k \tag{5.21}$$

$$\hat{y}_{k+1|k} = \hat{H}_{k+1} \hat{x}_{k+1|k} + J_{k+1} u_{k+1} \tag{5.22}$$

$$L_k = P_{k|k-1} H_k^T (H_k P_{k|k-1} H_k^T + R_k)^{-1} \tag{5.23}$$

$$\hat{x}_{k|k} = \hat{x}_{k|k-1} + L_k (y_k - H_k \hat{x}_{k|k-1}) \tag{5.24}$$

$$P_{k|k} = P_{k|k-1} - P_{k|k-1} H_k^T (H_k P_{k|k-1} H_k^T + R_k)^{-1} H_k P_{k|k-1} \tag{5.25}$$

The performance of the estimator can be judged by the error between the prediction the and actual measurement. The performance of the estimator can be seen in Figure 5.3.

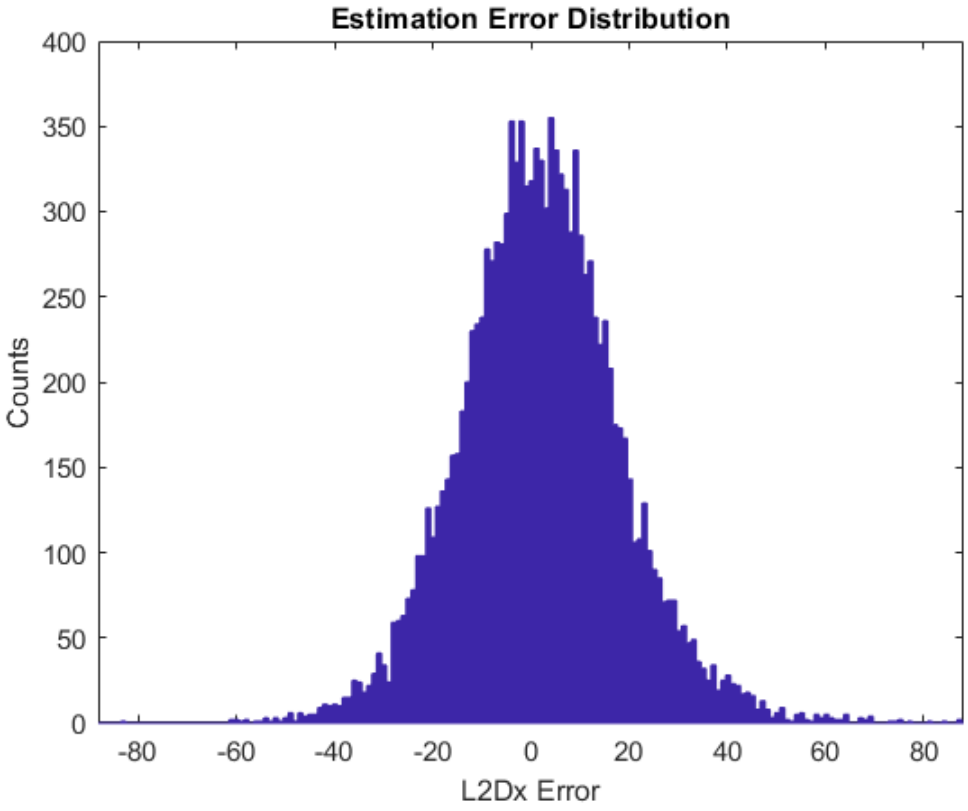

Figure 5.3: Distribution of error between L2Dx measurement and its one step ahead prediction

The error between the predicted and real L2Dx position has a mean of 2.0435 and has a standard distribution of 16.48. By plotting the normal probability of the error, it can be seen that error is approximately Gaussian (Figure 5.4).

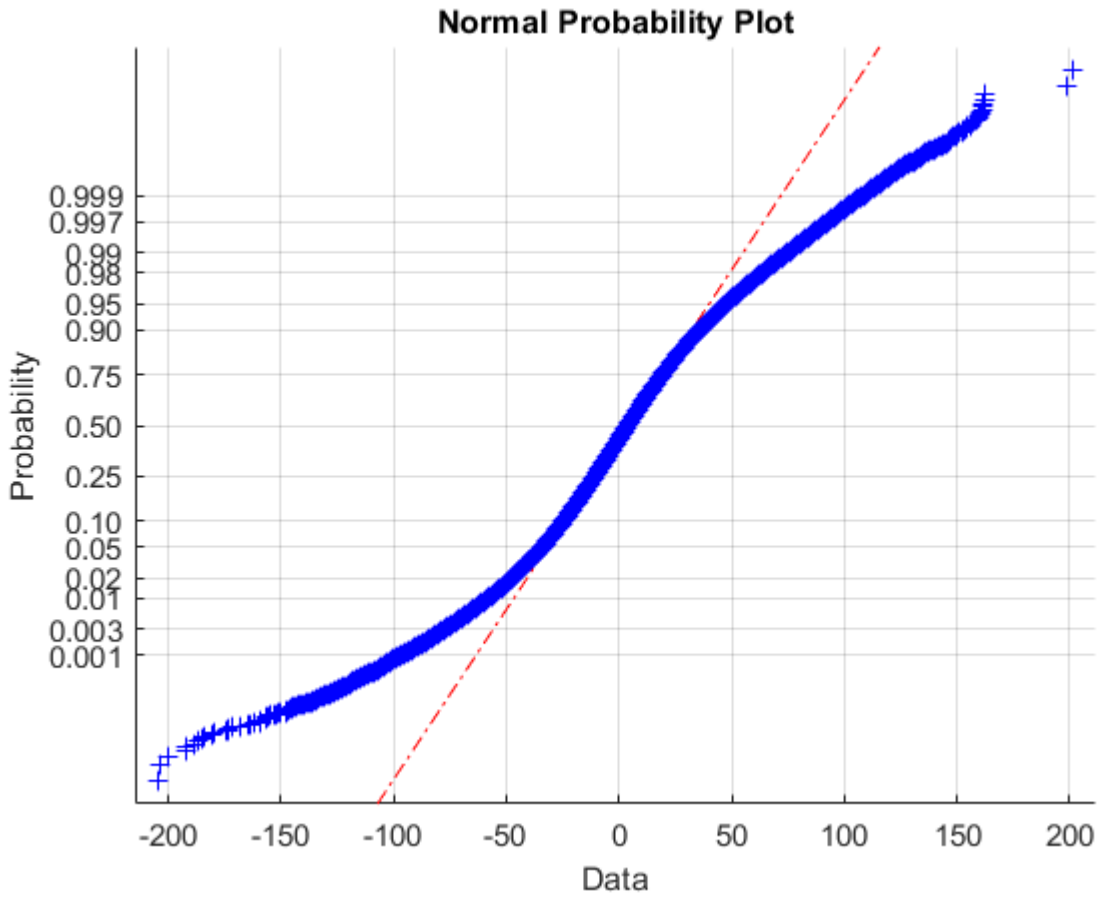

Figure 5.4: Estimator Error Normal Distribution

The estimator accurately predicts the position of the droplet within ±49.35. When compared to the process window of the t_{Fire} Scan, it can be seen that the error bounds keep the laser-to-droplet position within the acceptable range.

The performance of the estimator can be also evaluated by plotting the auto-correlation of the L2Dx measurement and the error between the L2Dx measurement and its one step ahead prediction. If the estimator is able to perfectly estimate the droplet position, the error would be white noise. In the normalized auto-correlation plot (Figure 5.5), the periodic spikes are due to the repetitive nature of the pulsing

experiment. The spikes indicate the uncertainty of the L2Dx position at the start of the packet. With the Kalman predictor, these spikes are greatly diminished.

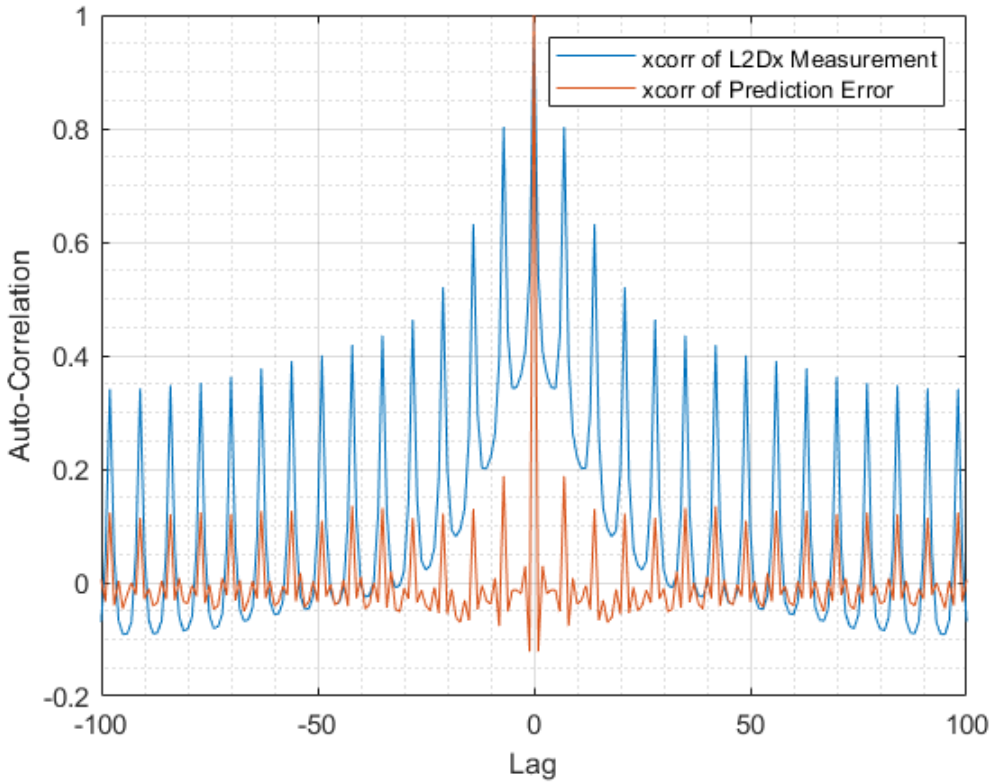

Figure 5.5: The Auto-Correlation of the L2Dx measurement (blue signal) is divided by its variance (2944.16) and the Prediction error (orange signal) is divide by its variance (271.14). Note that the variance is reduced indicating that the one-step ahead prediction is able to estimate the disturbance. Additionally, it can be seen that the algorithm whitens the noise.

By also plotting the normalized auto-correlation of the estimator error, it is observed that the spikes due to the Local Force are much smaller in magnitude. However, because the estimator is not able to perfectly predict the droplet position, there are still some periodic spikes in the auto-correlation plot. Periodic spikes are still present in the auto-correlation as the estimator is unable to perfectly predict the

droplet position. However, because the error is less than the size of the process window (± 150), the estimator fulfills its requirements.

Chapter 6

Conclusion

6.1 Summary

In this thesis, we have analyzed the operations of the EUV light source and investigated the dynamic properties of the Local Force. This information was then used to design a feedforward controller that can compensate for the disturbances caused by the Local Force when EUV is produced. Using data from a real system, a high-Fidelity simulation was designed, which shows that the feedforward controller was able to successfully reject the Local Force disturbance caused by EUV production.

In Chapter 2, the design and operation of the EUV source was introduced. First the concept of the main-pulse and the pre-pulse lasers was presented along with timing controls needed to accurately hit the droplet and produce stable EUV. Secondly, it was shown how the Local Force can disturb the upstream droplets and in turn have an effect on the EUV that is produced.

In Chapter 3, the various sensors, which can be used for measuring the impact of the local force, were introduced. The quadcells can used to measure the droplet displacement caused by the Local Force event as they are used to measure the position of the pre-pulse beam. The EUV photodiodes can be used to measure the amount

of EUV energy produced by the Local Force Event.

In Chapter 4, a series of experiments was proposed which would characterize the Local Force and provide the necessary information to construct a model of the Local Force. From these experiments, the following results were found:

- In L2Dx space, there is a region of 300 units where the Dose Error is less than 1%. Hence the estimator must have an error of less than ± 150 to fit within with the process window.
- The Local Force grows at a different rate from the Local Force decay, therefore the state estimation model changes depending on whether the droplet was hit or missed.
- The Local Force mostly dissipates after 3 droplets so the model only needs to keep a record of the past 3 droplets
- There is a delay between t_{Fire} and L2Dx and there are no additional dynamics. Therefore the test shows that the droplets are traveling at a constant speed.

In Chapter 5, a feedforward controller was developed using the modeling done in Chapter 4. To validate the controller, as high-fidelity simulation was created which executed at the same rate as the source. Using real data collected from the source, it was seen the 3 sigma error is ± 49.40, which is within the operating window.

6.2 Future Work

From the results of Chapter 4 and 5, it is seen that there is substantial error which has not been accounted. This maybe a result of other physical process or variables that were not explored in this thesis. Further research would investigate these factors and potentially building a more complex model.

At the time of writing this thesis the hardware and firmware required, to execute the algorithm described in this thesis within the required time, was not available. In the coming months and years, this technology will be implemented. At such time, this algorithm can be tested in practice and the performance can be further validated.

Bibliography

[1] W. A. Coppel, editor. *Mathematical control theory: proceedings, Canberra, Australia, August 23-September 2, 1977*, volume 680, chapter 2. Minimum Variance Control. Springer-Verlag, 1978.

[2] L. Guo, H. Huang, X. Wang, and D. Zhang. Exposure dose control for step-and-scan lithography. In Y. Wang, J. en Yao, and C. J. Progler, editors, *Advanced Microlithography Technologies*, volume 5645, pages 217 – 222. International Society for Optics and Photonics, SPIE, 2005.

[3] R. E. Kalman. A new approach to linear filtering and prediction problems" transaction of the asme journal of basic. 1960.

[4] L. Ljung. *System Identification: Theory for the User*, chapter 6. Nonparametric Time- amd Frequency-Domain Methods. Prentice Hall PTR, 2007.

[5] Lord Rayleigh. XXXI. Investigations in optics, with special reference to the spectroscope. *The London, Edinburgh, and Dublin Philosophical Magazine and Journal of Science*, 8(49):261–274, 1879.

[6] M. Purvis, I. V. Fomenkov, A. A. Schafgans, P. Mayer, K. Hummler, M. H. Leenders, Y. Tao, S. I. Rokitski, J. Stewart, A. I. Ershov, R. J. Rafac, S. D. Dea, G. O. Vaschenko, D. C. Brandt, and D. J. Brown. Laser-produced plasma incoherent EUV light sources for high-volume manufacturing semiconductor lithography (Conference Presentation). In A. Klisnick and C. S. Menoni, editors, *X-Ray Lasers and Coherent X-Ray Sources: Development and Applications XIII*, volume 11111. International Society for Optics and Photonics, SPIE, 2019.

[7] L. Salles and D. W. De Lima Monteiro. Designing the response of an optical quad-cell as position-sensitive detector. *Sensors Journal, IEEE*, 10:286 – 293, 03 2010.

[8] D. Simon. *Optimal State Estimation*, chapter 5. The discrete-time Kalman Filter. Wiley-Interscience, 2006.